Magnetotransport properties and magnetostructural phenomenon in single crystals of $La_{0.7}(Ca_{1-y}Sr_y)_{0.3}MnO_3$

Y. Tomioka,[1] A. Asamitsu,[1,*] and Y. Tokura[1,2]
[1]*Joint Research Center for Atom Technology (JRCAT), 1-1-4 Higashi, Tsukuba 305-0046, Japan*
[2]*Department of Applied Physics, University of Tokyo, 7-3-1 Hongo, Tokyo 113-0033, Japan*
(Received 27 March 2000; revised manuscript received 24 July 2000; published 19 December 2000)

The magnetotransport and magnetostructural properties of $La_{0.7}(Ca_{1-y}Sr_y)_{0.3}MnO_3$ ($0 \leqslant y \leqslant 1$) are studied. We investigate the variation in magnetoresistance (MR) with y and the field-induced structural transition at $y \sim 0.5$ by using single crystals prepared by the floating-zone method. With the increase in y, the colossal MR behavior at $y \sim 0$ is transformed to a rather canonical MR (a MR free from lattice effects) at $y=1$. The coefficient C in the empirical relation that $\rho(M)/\rho(0) = \exp[-C(M/M_s)^2]$ (M and M_s being the magnetization and its zero-temperature saturation value) shows a significant change with y, attainable for example, from 7.6 at $y=0.1$ to 2.3 at $y=0.7$. As an example of the magnetoswitching of a crystal structure around room temperature, the structural-phase transition induced by an external magnetic field is investigated for crystals with $y \sim 0.5$. Structural-phase diagrams of the magnetic field vs temperature plane are given.

DOI: 10.1103/PhysRevB.63.024421 PACS number(s): 75.60.−d, 71.27.+a, 71.30.+h

I. INTRODUCTION

Manganese oxides with perovskite structures show versatile phenomena due to a close interplay among the spin, charge, and orbital (lattice), which show up as magnetostructural phenomena,[1–3] colossal magnetoresistance (CMR),[4] and melting of charge/orbital ordering in magnetic fields,[5,6] for example. A key parameter in controlling the physical properties of these materials is the transfer interaction of an e_g-orbital carrier between the neighboring Mn sites. In $R_{1-x}A_xMnO_3$ (R and A being rare-earth and alkaline-earth elements, respectively), a lattice distortion, or a tilting of MnO_6 octahedra, depends on the averaged ionic radius of R and A cations. The (R, A)-site composition controls an effective one-electron bandwidth W, because with a smaller averaged radius of the (R, A) site the transfer interaction of an e_g-orbital electron becomes smaller in a network of MnO_6 octahedra. In $La_{1-x}Sr_xMnO_3$ ($x > 0.3$), a typical example with a relatively large W,[7] the e_g-orbital carriers tend to be itinerant, and due to the strong ferromagnetic interaction (Hund's-rule coupling, J_H) between local t_{2g} and itinerant e_g electrons, the ferromagnetic and metallic state is stabilized.[8,9] The ferromagnetic and metallic state has been well interpreted by the double-exchange (DE) mechanism.[10–12] When the W is narrowed, on the other hand, the DE ferromagnetism suffers from other competing instabilities, e.g., an antiferromagnetic interaction between local t_{2g} spins, charge/orbital ordering, and electron-lattice coupling (collective Jahn-Teller distortions).[13] In a distorted perovskite manganite, $Pr_{1-x}Ca_xMnO_3$ ($0.3 \leqslant x < 0.75$), for example, charge/orbital ordering overcomes the ferromagnetic and metallic state,[14,15] and the ground state is an antiferromagnetic insulating state.

In this paper we report on the magnetotransport properties and magnetostructural phenomenon in single crystals of $La_{0.7}(Ca_{1-y}Sr_y)_{0.3}MnO_3$, in which the W is increased by substitution of Ca with Sr, while the hole-doping level ($x = 0.3$) used to maximize T_C is kept constant. We demonstrate the variation of magnetotransport with y, that is, from a typical CMR behavior at $y=0$ to a rather canonical MR (the MR free from lattice effects[16]) at $y=1$. In the canonical MR, as indicated in Ref. 16, the magnitude is dependent only on the density of conduction carriers (n) as such a manner that $C \propto n^{-2/3}$ in the approximation of $\Delta\rho/\rho = C(M/M_s)^2$ (M_s being a saturation magnetization). Another issue described in this paper is the magnetic-field-induced structural transition as a close interplay among the spin, charge, and lattice.[17,18] $La_{0.7}(Ca_{1-y}Sr_y)_{0.3}MnO_3$ undergoes a structural transition between orthorhombic and rhombohedral structures as the temperature varies.[19,20] At $y \sim 0.5$, both the temperatures of the ferromagnetic transition (T_C) and structural transition (T_S) are so close around room temperature that the structural transition can be induced by application of an external magnetic field.

The experimental procedures, including preparation of $La_{0.7}(Ca_{1-y}Sr_y)_{0.3}MnO_3$ crystals by the floating-zone method, are first described in Sec. II. In Sec. III, an overview of the electronic- (and structural-) phase diagram and magnetotransport properties are presented. In Sec. IV, a structural transition for $y \sim 0.5$ induced by an external magnetic field is presented. For a crystal with $y \sim 0.5$, a structural-phase diagram is demonstrated on the magnetic field vs temperature plane. A summary is given in Sec. V.

II. EXPERIMENTAL PROCEDURES

Single crystals of $La_{0.7}(Ca_{1-y}Sr_y)_{0.3}MnO_3$ were prepared by the floating-zone method. Powders of La_2O_3, $SrCO_3$, $CaCO_3$, and Mn_3O_4 were mixed at the prescribed ratio and calcined in air at 1200 °C for 24–48 h. The obtained powders were then pressed into a rod 5 mm in diameter and 80 mm in length. The rod was then sintered in air at 1350–1450 °C for 30 h. Crystal was grown in a stream of air at a growth rate of 3–10 mm/h with rotating feed and seed rods in opposite directions. (For $y < 0.3$ the growth rate was set at less than 5 mm/h because a faster growth rate was not successful for the formation of the single crystal.) Part of the crystal boule was

TABLE I. Results of analysis of the compositions for single crystals of $La_{1-x}(Ca_{1-y}Sr_y)_xMnO_3$ prepared by the floating-zone method with the prescribed compositions $x=0.30$ and $y=0-1$.

y (nominal)	x (Ca+Sr/La+Ca+Sr)	y Sr(Ca+Sr)	T_c (K)	$M_s(\mu_B$/ Mn site)[a]	Crystal system[b]	ρ_0 ($\mu\,\Omega$ cm)[c]
0	0.274	0.000	223	3.31	ortho.	143
0.1	0.303	0.105	240	3.36	ortho.	153
0.3	0.286	0.313	278	3.34	ortho.	154
0.45	0.295	0.450	309	3.45	ortho.	160
0.5	0.299	0.507	326	3.46	ortho.	112
0.55	0.306	0.542	331	3.46	rhombo.	127
0.7	0.298	0.711	341	3.46	rhombo.	71.9
1.0	0.300	1.000	369	3.50	rhombo.	45.1

[a]The saturation magnetization M_s measured at 5 K and 0.5 T.
[b]The crystal system at room temperature (300 K).
[c]The residual resistivity at 10 K.

pulverized and characterized by powder x-ray diffraction, which confirmed that the melt-grown crystal was single phase. Lattice parameters and crystal structures were examined by Rietveld refinement of the diffraction pattern. The formation of the single crystal was also confirmed by an x-ray Laue reflection method. The cation ratios analyzed by inductively coupled plasma spectroscopy are listed in Table I together with the ferromagnetic transition temperature, the saturation magnetization, the crystal system at room temperature, and the residual resistivity for $La_{0.7}(Ca_{1-y}Sr_y)_{0.3}MnO_3$. As Table I indicates, the analyzed ratio of Ca/(La+Ca+Sr) for $y=0$ was slightly but distinctly smaller than the prescribed one, which suggests that an incongruent melting occurs upon substitution of La by Ca in a melt-grown process. For $y>0.3$, however, the analyzed cation ratio coincides with the prescribed one, and the deficiency of Ca in a melt-grown crystal disappears, as indicated in Table I. The observed T_C for the $y=0$ single crystal is distinctly lower by about 15 K than those of the corresponding polycrystal reported in the literature.[21] Off-stoichiometry of the oxygen content from 3.0 might reduce the T_C of a $y=0$ crystal,[22,23] although the apparent oxygen nonstoichiometry was not detected for the present $x=0.3$, $y=0$ single crystal.[24]

The magnetization was measured by using a superconducting quantum interference device magnetometer. The resistivity in the magnetic field was measured by using a superconducting magnet up to 7 T employing a standard four-probe method with the current parallel to the direction of the external magnetic field.

III. MAGNETOTRANSPORT PROPERTIES

Figure 1 shows a magnetic- and structural-phase diagram of $La_{0.7}(Ca_{1-y}Sr_y)_{0.3}MnO_3$. As y increases, the ferromagnetic transition temperature T_C increases, while the structural transition temperature T_S decreases. The T_C and T_S cross each other at $y\sim0.5$. For $y>0.5$, T_S immediately decreases with the increase in y, and goes to zero at $0.5<y<0.55$. The T_C depends almost linearly on y, although dT_C/dy in the orthorhombic (O) region ($y<0.5$) is steeper than that in the rhombohedral (R) one ($y>0.5$). As a result, a discontinuity in $T_C(y)$ is clearly seen at $y\sim0.5$.

Figure 2 shows the temperature profiles of the resistivity ρ (lower panel) and $(d\rho/dT)/\rho$ (upper panel) for $La_{0.7}(Ca_{1-y}Sr_y)_{0.3}MnO_3$ crystals with varying y. The anomaly at $\sim$370 K in the resistivity of the $y=0.45$ crystal is due to a structural transition between the O and the R phase. T_C is manifested as a peak in the $(d\rho/dT)/\rho$ curve or a decrease in resistivity, and increases with the increase in y. The singular-peak feature in the $(d\rho/dT)/\rho$ curve for low-y (Ca-rich) crystals indicates the almost discontinuous (first-order-like) phase change. The transition becomes more gradual with increasing y. Because lattice distortion decreases and the Mn-O-Mn bond angle increases (or W in-

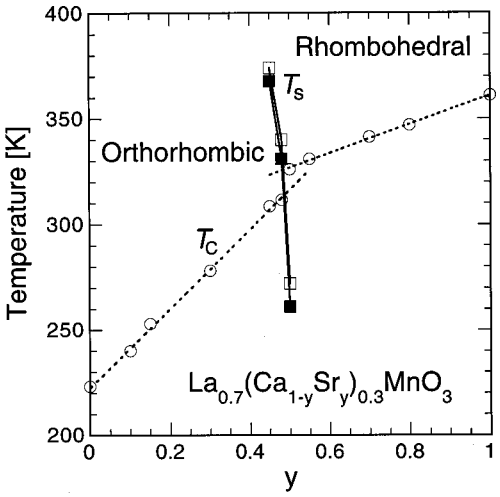

FIG. 1. An electronic- as well as structural-phase diagram for $La_{0.7}(Ca_{1-y}Sr_y)_{0.3}MnO_3$. The ferromagnetic transition temperature T_C is denoted by open circles, while the structural transition temperature T_S in the temperature-increasing and -decreasing runs are denoted by open and closed squares, respectively. The y dependence of T_C is approximated by the relations $T_C(y)=222.3\,\mathrm{K}+(188.1\,\mathrm{K})y$ ($0<y<0.5$ in the orthorhombic form) and $282.9\,\mathrm{K}+(85.6\,\mathrm{K})y$ ($0.5<y<1$ in the rhombohedral form), which are denoted by dashed lines.

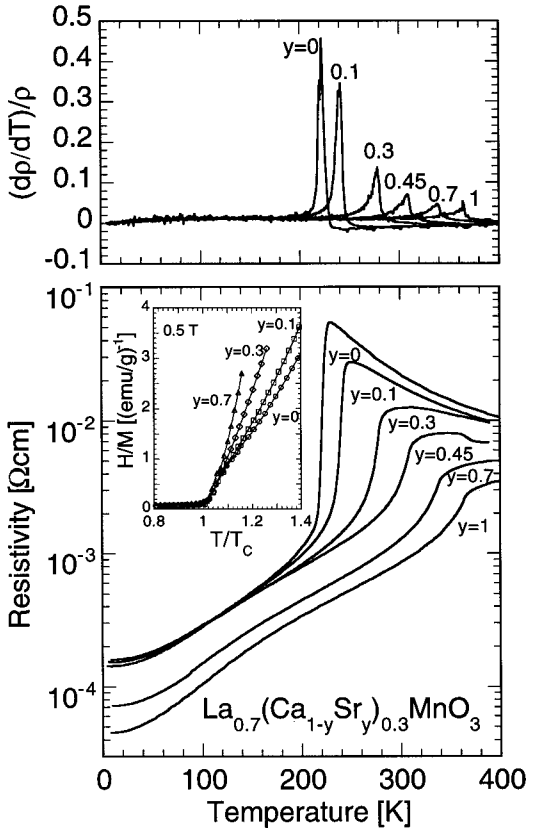

FIG. 2. (a) Temperature profiles of $(d\rho/dT)/\rho$ for various $La_{0.7}(Ca_{1-y}Sr_y)_{0.3}MnO_3$ crystals. The ferromagnetic transition temperature is manifested as a peak of $(d\rho/dT)/\rho$. (b) Temperature profiles of resistivity for $La_{0.7}(Ca_{1-y}Sr_y)_{0.3}MnO_3$ crystals with varying y. The anomaly at ~370 K for the resistivity of the $y=0.45$ crystal is due to a structural transition between orthorhombic (low-temperature) and rhombohedral (high-temperature) phases. The inset shows inverse susceptibility vs T/T_C for $y=0$, 0.1, 0.3, and 0.7 crystals.

creases) with Sr doping, the DE interaction is strengthened and the ferromagnetic and metallic state is stabilized with the increase in y. In other words, other competing instabilities against the DE interaction become relevant with the decrease in y. Correspondingly, the deviation in inverse susceptibility from the Curie-Weiss law is pronounced with a decrease in y, as shown in the inset of the lower panel in Fig. 2. These features suggest that an antiferromagnetic interaction exists just above T_C for $y\sim 0$. Another noteworthy aspect of Fig. 2 is that the resistivity at the lowest temperature takes almost the same value for $0\leqslant y\leqslant 0.45$ where the crystal structure is orthorhombic, while it decreases with the increase in y for $y\geqslant 0.7$ where the crystal structure is rhombohedral.

Figure 3 shows the temperature profiles of resistivity in magnetic fields for $y=0$ ($La_{0.7}Ca_{0.3}MnO_3$) and $y=1$ ($La_{0.7}Sr_{0.3}MnO_3$) crystals. The anomalously large MR or CMR at $y=0$ is transformed to a rather canonical MR at $y=1$. The variation in the magnetotransport property with y, as shown in Fig. 3, is further quantified by isothermal measurements of magnetization and resistivity in magnetic fields. Figure 4 shows the normalized resistivity as a function of the

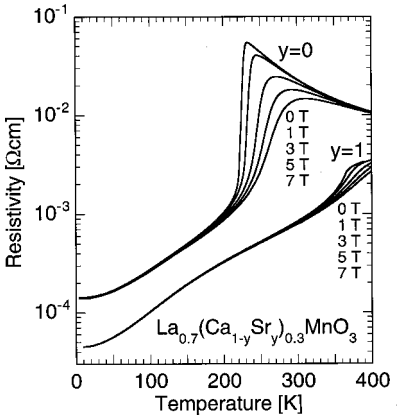

FIG. 3. Temperature profiles of resistivity in several magnetic fields for $y=0$ ($La_{0.7}Ca_{0.3}MnO_3$) and $y=1$ ($La_{0.7}Sr_{0.3}MnO_3$) crystals, as the prototypes of the bandwidth-controlled system of $La_{0.7}(Ca_{1-y}Sr_y)_{0.3}MnO_3$. The anomalously large MR or CMR at $y=0$ is transformed to a rather canonical MR at $y=1$.

square of reduced magnetization (M/M_s) for $y=0.1$, 0.3, and 0.7 crystals, which are taken just above T_C ($1.02T_C < T < 1.17T_C$). As indicated by the broken lines, the MR magnitude $\rho(M)/\rho(0)$ is well approximated over a fairly large M region by the following empirical relation:[25,26]

$$\rho(M)/\rho(0)=\exp[-C(M/M_s)^2]. \tag{1}$$

This formula was originally proposed assuming that the resistivity in a ferromagnetic semiconductor obeys the thermal-activation-type law, and that the activation energy is reduced in proportion to M^2.[25,26] In Ref. 26, Bebenin and Ustinov applied this formula to the MR of low-doped semiconducting $La_{1-x}Sr_xMnO_3$ Refs. 8 and 9 by assuming that the mobility edge present within the conduction band shows the energy

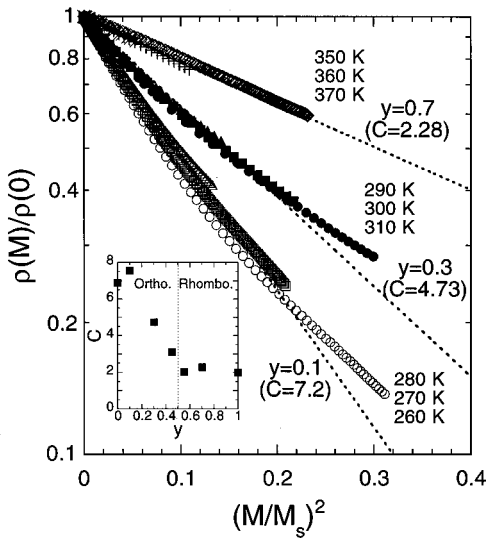

FIG. 4. Normalized resistivity on a logarithmic scale as a function of the square of reduced magnetization for $y=0.1$, 0.3, and 0.7 crystals of $La_{0.7}(Ca_{1-y}Sr_y)_{0.3}MnO_3$. The $\rho(M)/\rho(0)$ was analyzed by using Eq. (1) (see text), and the variation of C (a slope of this plot) with y is shown in the inset.

shift in proportion to M^2. In reality, such an activation-type behavior can be seen for $y<0.3$, but not for $y>0.5$, and the starting assumption for Eq. (1) is not everywhere valid for the present series of crystals. Nevertheless, this empirical formula reproduces well the MR behavior with $C=2-7$ for the region of $(M/M_s)^2 \leqslant 0.2$. In Ref. 27, the coefficient C is further related with the magnetic barrier contribution in a theoretical model[28] based on variable range hopping with barriers due to magnetic disorder.

The variation of the coefficient C with y is shown in the inset of Fig. 4. The C value shows a distinct decrease for $0<y<0.5$ where the crystal structure is orthorhombic, while it is almost constant (~ 2) for $0.5<y<1$ where the crystal structure is rhombohedral. (A nonsystematically larger C value at $y=0.1$ than at $y=0$ may be due to an effect of the local disorder by a distinct difference of ionic radii between Sr and Ca.) According to the theory by Furukawa,[29,30] the coefficient C [in the low M/M_s region, namely, in the region where $\rho(M)/\rho(0)=1-C(M/M_s)^2$] depends on the ratio of J_H/W and can increase from unity in a weak-coupling limit ($J_H/W\sim 1$) to 4 in a strong-coupling regime ($J_H/W \gg 1$). In $La_{0.7}(Ca_{1-y}Sr_y)_{0.3}MnO_3$, as shown in the inset, a C value lower than 4 is seen for $y>0.3$. Considering that the above-T_C resistivity shows a metallic temperature dependence in the rhombohedral region (see Fig. 1), the MR with $C\sim 2$ for $y>0.5$ is considered as the canonical MR,[16] and can be basically interpreted in the framework of the DE model.[29,30] For $y<0.3$, on the other hand, other explicit factors are needed to interpret the huge MR effect with $C>4$. As a possible cause of the CMR effect for $y<0.3$, a Jahn-Teller-type electron-lattice coupling on the transport properties[16,31] may be considered. In other prototypical CMR systems, such as $(Nd,Sm)_{0.5}Sr_{0.5}MnO_3$ $(x=0.5)$,[32] $Sm_{0.55}Sr_{0.45}MnO_3$ $(x=0.45)$,[33] and $La_{1.2}Sr_{1.8}Mn_2O_7$ $(x=0.4)$,[34] strong x-ray diffuse scattering features with incommensurate peaks have been observed above T_C, indicating the short-range orbital/charge order or the spatial correlation of Jahn-Teller polarons. Although a concrete pattern of orbital ordering is not clear for the present lower-doped case, these features imply that a strong charge/orbital correlation coupled with local lattice distortion as well as macroscopic lattice strain and its field-induced suppression are responsible for such a large coefficient C or CMR.

IV. STRUCTURAL TRANSITION INDUCED BY AN EXTERNAL MAGNETIC FIELD

As shown in Fig. 1, the transition temperatures T_C and T_S become comparable around $y\sim 0.5$. In this compositional region, the coupling among spin, charge, and lattice becomes so strong that application of an external magnetic field can induce a structural transition. Figure 5 shows the temperature profiles of resistivity at 0 and 3 T for a $y=0.47$ crystal ($T_C\sim 303$ K), and the inset exemplifies the most hysteretic resistivity at 1 T. At 0 T, T_S locates at 323 and 331 K in both cooling and warming runs, respectively, while at 3 T it decreases to 269 and 284.5 K, respectively. As shown in the data at 3 T, the application of an external magnetic field decreases the resistivity near T_C in terms of the reduced spin

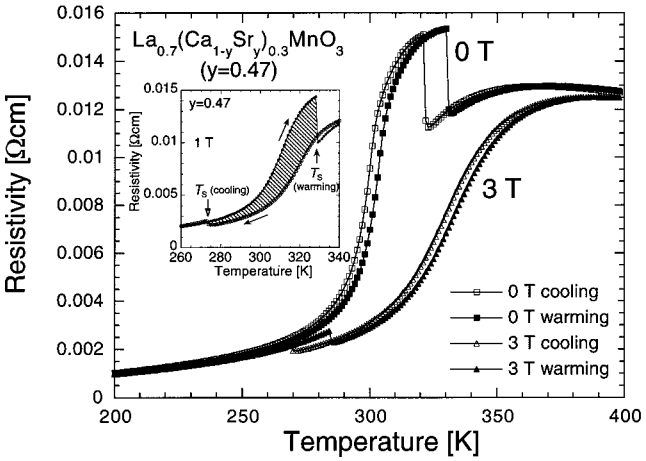

FIG. 5. Temperature profiles of resistivity at 0 and 3 T for a $y=0.47$ crystal ($T_C\sim 303$ K). Open and closed symbols indicate cooling and warming runs, respectively. The inset shows temperature profiles of resistivity at 1 T of the same crystal.

scattering of conduction carriers. Such a field-induced low-resistive state may stabilize a rhombohedral structure, resulting in a decrease in T_S ($<T_C$) at 3 T. The thermal hysteresis of T_S is most pronounced at 1 T, which is indicated by the hatched area in the inset. Due to the enhanced first-order nature of the structural transition via coupling with the magnetic transition, T_S in the cooling run decreases down to ~ 274 K, while that in the warming run increases up to ~ 329 K. For $y<0.47$ and $y\geqslant 0.5$, the structural transition temperatures are too high and low, respectively, to induce a field-induced structural transition (at least for $\mu_0 H<7$ T).

For a $y=0.47$ crystal, the structural transition induced by an external magnetic field has further been confirmed by isothermal resistivity in magnetic fields. Figure 6 shows (a) the magnetization and (b) the resistivity for a $y=0.47$ crystal taken at 290, 305, and 325 K. At 305 K, steep changes in magnetization are observed at $\mu_0 H=1.4$ and 0.5 T in field-increasing and field-decreasing runs, respectively. In accord with the changes in magnetization, a resistivity drop and jump are seen at the corresponding magnetic fields [Fig. 6(b)]. Since the crystal structure at 305 K for $y=0.47$ is orthorhombic at zero magnetic field, the application of an external magnetic field causes an *O*-to-*R* transition. Another noteworthy aspect of Fig. 6 is that the field-induced transition becomes irreversible in a restricted temperature region because of the first-order nature of the transition. In the case of the runs at 325 K, the sample was first cooled below the structural transition temperature (e.g., to 250 K), and then the temperature was raised to 325 K. At this stage, the *O* structure is maintained as the superheated state (see also Fig. 5). Then, application of an external magnetic field causes an *O*-to-*R* transition at ~ 1.3 T in the field-increasing run. In the subsequent field-decreasing run, however, the *R* structure is kept down to zero field as the supercooled state because the temperature of 325 K at zero field is in the hysteresis region, as indicated in Fig. 5. Also at 290 K, an irreversible transition from *O* to *R* structure occurs at about 1.5 T in the field-

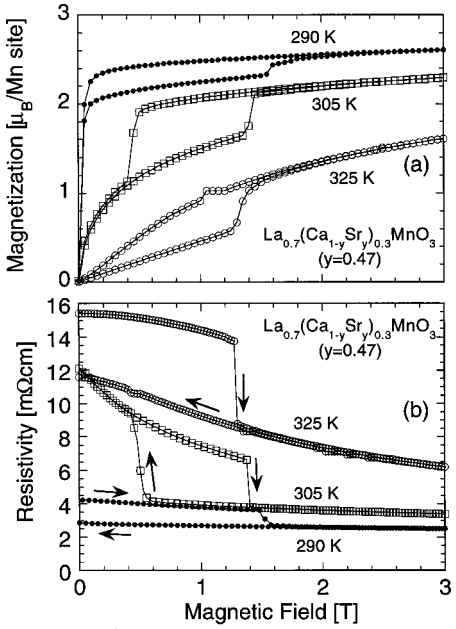

FIG. 6. (a) Magnetization and (b) resistivity at 290, 305, and 325 K for a $y=0.47$ crystal. In the experimental run at 325 K, the sample was first cooled below the structural transition temperature, and then the temperature was raised to 325 K. Irreversible behavior is seen in the data at 290 and 325 K.

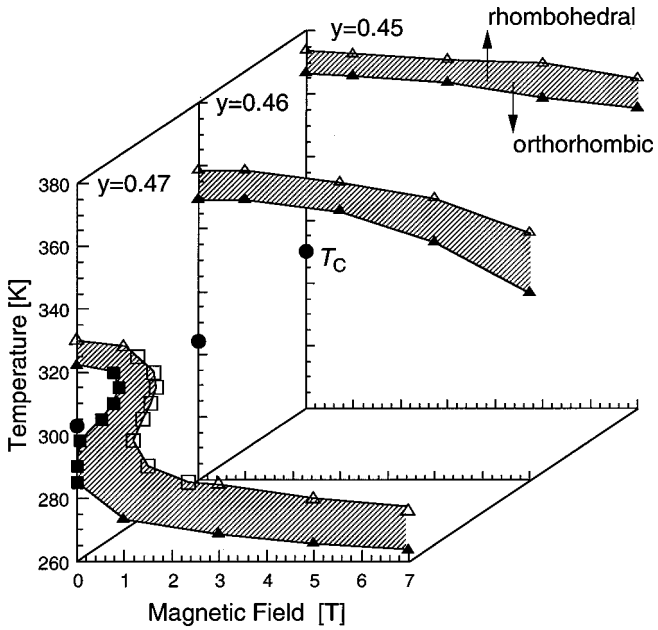

FIG. 7. Structural-phase diagrams of $y=0.45$, 0.46, and 0.47 crystals in magnetic field vs temperature planes. The hysteresis region is shown by the hatched area. The critical temperatures (magnetic fields) from an orthorhombic to a rhombohedral structure and vice versa are denoted by open and closed triangles (squares), respectively, which are determined by the temperature dependence of resistivity in respective magnetic fields (field dependence of isothermal resistivity at respective temperatures). Closed circles indicate Curie temperatures.

increasing run. However, this irreversibility is likely due to the supercooling effect characteristic of the field-induced first-order transition.

These measurements of the field-induced structural transition provide the structural phase diagram of the magnetic field vs temperature plane shown in Fig. 7 for the $y=0.45$, 0.46, and 0.47 crystals. The hysteresis region is shown by the hatched area. With the increase in y from 0.45 to 0.46 in this figure, the decrease in T_S in the magnetic fields seems to be pronounced. For $y=0.45$ and 0.46, however, T_S is always higher than T_C at least for $\mu_0 H \leqslant 7$ T. For $y=0.47$, on the other hand, the *O*-*R* transition temperature decreases from $\sim$330 K at 0 T to $\sim$275 K at 7 T, showing a steep change at $1\ \mathrm{T} < \mu_0 H < 1.5\ \mathrm{T}$. In Fig. 7, a temperature hysteresis exists between 327 and 337 K at zero field, and a field-scanning process at 325 K, thus traces a hysteresis region below about 1.2 T. As a result, an irreversible feature is seen as shown by the data at 325 K in Fig. 6.

The coupled phenomenon among spin, charge, and lattice as shown in Fig. 7 is quantitatively explained by a Landau free-energy expansion with coupled order parameters, magnetization (M), and lattice distortion (Q).[35] Phenomenologically, a transition from *O* to *R* structure in magnetic fields takes place due to a free-energy gain in the Zeeman-term MH, since magnetization in the *R* phase is larger than that in the *O* structure. A magnetostructural phenomenon similar to that in $La_{1-x}Sr_xMnO_3$ ($x\sim0.17$) (Refs. 1 and 2) has thus been confirmed as an even more pronounced feature around room temperature in the system of $La_{0.7}(Ca_{1-y}Sr_y)_{0.3}MnO_3$ ($y\sim0.5$).

V. SUMMARY

We have studied magnetotransport properties and the field-induced phenomenon for the system of $La_{0.7}(Ca_{1-y}Sr_y)_{0.3}MnO_3$. By utilizing single-crystal samples, we have investigated the variation in MR with y and the field-induced structural transition attained at $y\sim0.5$. With an increase in y, the CMR behavior at $y\sim0$ is transformed to a rather canonical MR (the MR free from lattice effects) at $y=1$. The coefficient C in the empirical relation that $\rho(M)/\rho(0)=\exp[-C(M/M_s)^2]$ was estimated for several crystals with varying y. The C value decreases with y, say from 7.6 at $y=0.1$ to 2.3 at $y=0.7$. For a $y=0.47$ crystal, we have demonstrated the structural-phase transition induced by an external magnetic field. Structural-phase diagrams of $y=0.45$, 0.46, and 0.47 crystals around room temperature were obtained on the magnetic field vs temperature planes.

ACKNOWLEDGMENTS

This research was supported by NEDO (New Energy and Industrial Technology Development Organization of Japan) and was carried out under the joint research agreement between the National Institute for Advanced Interdisciplinary Research (NAIR) and the Angstrom Technology Partnership (ATP). The authors thank T. Okuda of JRCAT for helpful discussions.

*Present address: Cryogenic Center, University of Tokyo, Tokyo 113-0032, Japan.
[1] A. Asamitsu, Y. Moritomo, Y. Tomioka, T. Arima, and Y. Tokura, Nature (London) **373**, 407 (1995).
[2] A. Asamitsu, Y. Moritomo, R. Kumai, Y. Tomioka, and Y. Tokura, Phys. Rev. B **54**, 1716 (1996).
[3] J. M. De Teresa, M. R. Ibarra, J. Blasco, J. Garcia, C. Marquina, P. A. Algarabel, Z. Arnold, K. Kamenev, C. Ritter, and R. von Helmolt, Phys. Rev. B **54**, 1187 (1996).
[4] For instance, see K. Chahara, T. Ohno, M. Kasai, and Y. Kozono, Appl. Phys. Lett. **63**, 1990 (1993); R. von Helmolt, J. Wecker, B. Holzapfel, M. Schultz, and K. Samwer, Phys. Rev. Lett. **71**, 2331 (1993); S. Jin, T. H. Tiefel, M. McCormack, R. A. Fastnacht, R. Ramesh, and L. H. Chen, Science **264**, 413 (1994); H. L. Ju, C. Kwon, R. L. Green, and T. Venkatesan, Appl. Phys. Lett. **65**, 2108 (1994).
[5] H. Kuwahara, Y. Tomioka, A. Asamitsu, Y. Moritomo, and Y. Tokura, Science **270**, 961 (1995).
[6] Y. Tomioka, A. Asamitsu, Y. Moritomo, and Y. Tokura, J. Phys. Soc. Jpn. **63**, 1689 (1995).
[7] H. Y. Hwang, S. W. Cheong, P. G. Radaelli, M. Marezio, and B. Batlogg, Phys. Rev. Lett. **75**, 914 (1995).
[8] Y. Tokura, A. Urushibara, Y. Moritomo, T. Arima, A. Asamitsu, G. Kido, and N. Furukawa, J. Phys. Soc. Jpn. **63**, 3931 (1994).
[9] A. Urushihara, Y. Moritomo, T. Arima, A. Asamitsu, G. Kido, and Y. Tokura, Phys. Rev. B **51**, 14 103 (1995).
[10] C. Zener, Phys. Rev. **82**, 403 (1951).
[11] P. W. Anderson and H. Hasegawa, Phys. Rev. **100**, 675 (1955).
[12] P.-G. de Gennes, Phys. Rev. **118**, 141 (1960).
[13] Y. Tokura, H. Kuwahara, Y. Moritomo, Y. Tomioka, and A. Asamitsu, Phys. Rev. Lett. **76**, 3184 (1995).
[14] E. Pollert, S. Krupička, and E. Kuzmičová, J. Phys. Chem. Solids **43**, 1137 (1982).
[15] Z. Jirák, S. Krupička, Z. Šimša, M. Dlouhá, and S. Vratislav, J. Magn. Magn. Mater. **53**, 153 (1985).
[16] P. Majumdar and P. B. Littlewood, Nature (London) **395**, 479 (1998).
[17] S. Uhlenbruck, R. Teipen, R. Klingeler, B. Büchner, O. Friedt, M. Hücker, H. Kierspel, T. Niemöller, L. Pinsard, A. Revcolevschi, and R. Gross, Phys. Rev. Lett. **82**, 185 (1999).
[18] P. Wagner, I. Gordon, S. Mangin, V. V. Moshchalkov, Y. Bruynseraede, L. Pinsard, and A. Revcolevschi, Phys. Rev. B **61**, 529 (2000).
[19] P. G. Radaelli, M. Marezio, H. Y. Hwang, S-W. Cheong, and B. Batlogg, Phys. Rev. B **54**, 8992 (1996).
[20] P. G. Radaelli, M. Marezio, H. Y. Hwang, and S-W. Cheong, J. Solid State Chem. **122**, 444 (1996).
[21] S-W. Cheong and H. Y. Hwang, in *Colossal Magnetoresistive Oxides*, edited by Y. Tokura (Gordon and Breach, New York, 1999), p. 237.
[22] B. Dabrowski, P. W. Klamut, Z. Bukowski, R. Dybzinski, and J. E. Siewenie, J. Solid State Chem. **144**, 461 (1999).
[23] B. Dabrowski, R. Dybzinski, Z. Bukowski, O. Chmaissen, and J. D. Jorgensen, J. Solid State Chem. **146**, 488 (1999).
[24] T. Okuda, Y. Tomioka, A. Asamitsu, and Y. Tokura, Phys. Rev. B **61**, 8009 (2000).
[25] S. von Molnar and S. Methfessel, J. Appl. Phys. **38**, 959 (1967).
[26] N. G. Bebenin and V. V. Ustinov, J. Phys.: Condens. Matter **10**, 6301 (1998).
[27] P. Wagner, I. Gordon, L. Trappeniers, J. Vanacken, F. Herlach, V. V. Moshchalkov, and Y. Bruynseraede, Phys. Rev. Lett. **81**, 3980 (1998).
[28] M. Viret, L. Ranno, and J. M. D. Coey, Phys. Rev. B **55**, 8067 (1997).
[29] N. Furukawa, J. Phys. Soc. Jpn. **64**, 2734 (1995).
[30] N. Furukawa, J. Phys. Soc. Jpn. **64**, 2754 (1995).
[31] A. J. Millis, P. B. Littlewood, and B. I. Shraiman, Phys. Rev. Lett. **74**, 5144 (1995).
[32] S. Shimomura, N. Wakabayashi, H. Kuwahara, and Y. Tokura, Phys. Rev. Lett. **83**, 4389 (1999).
[33] E. Saitoh, Y. Tomioka, T. Kimura, and Y. Tokura, J. Phys. Soc. Jpn. **69**, 2403 (2000).
[34] D. N. Argyriou, H. N. Bordallo, J. F. Mitchel, J. D. Jorgensen, and G. F. Strouse, Phys. Rev. B **60**, 6200 (1999).
[35] Y. Imry, J. Phys. C **8**, 567 (1975).